Title
SARS-CoV-2 Infection Dysregulates the Metabolomic and Lipidomic Profiles of Serum

Journal
iScience, 23(10)

ISSN
2589-0042

Authors
Bruzzone, Chiara
Bizkarguenaga, Maider
Gil-Redondo, Rubén
et al.

Publication Date
2020-10-01

DOI
10.1016/j.isci.2020.101645

Peer reviewed

iScience

CellPress
OPEN ACCESS

Article

SARS-CoV-2 Infection Dysregulates the Metabolomic and Lipidomic Profiles of Serum

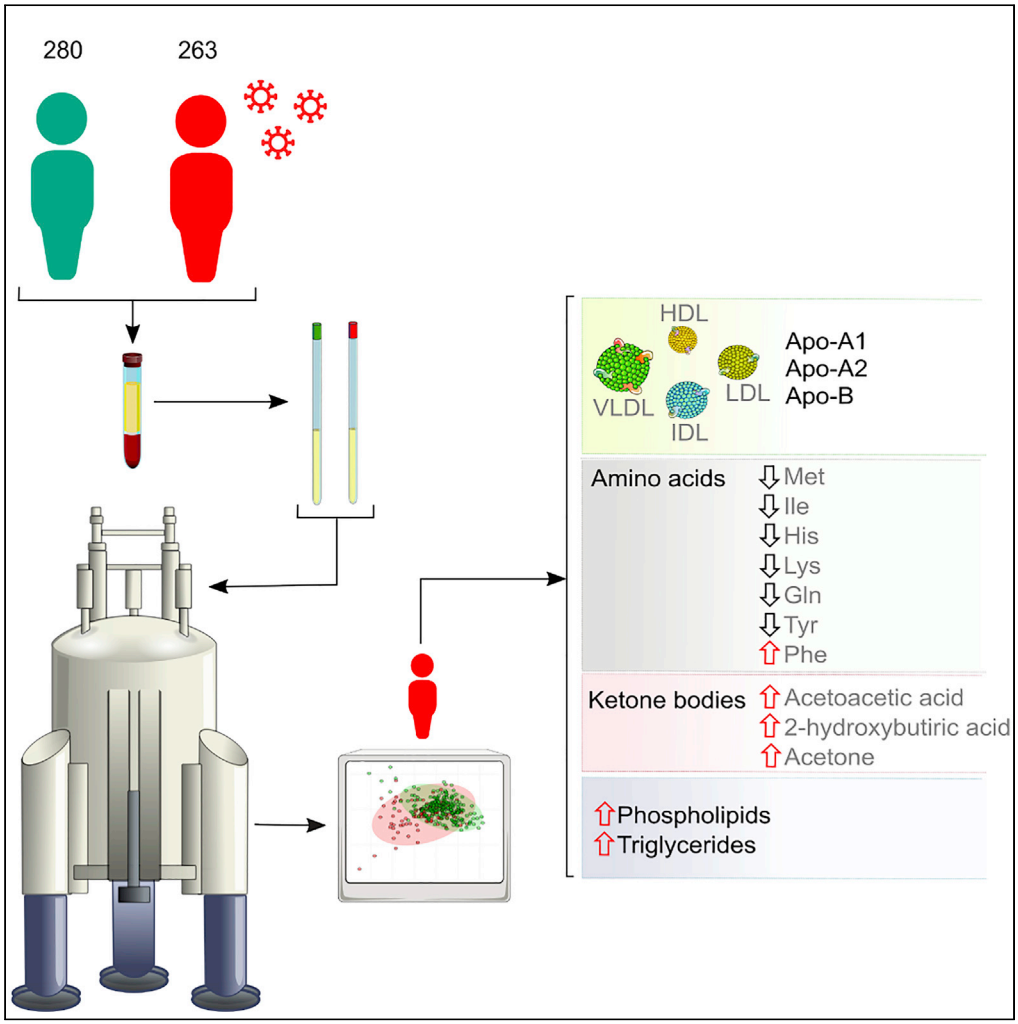

Chiara Bruzzone, Maider Bizkarguenaga, Rubén Gil-Redondo, ..., Shelly Lu, José M. Mato, Oscar Millet

omillet@cicbiogune.es

HIGHLIGHTS

Metabolomic and lipidomic serum profile of 398 COVID-19 acute-phase patients

Severe dyslipidemia that affects lipoprotein particle size and distribution

Central metabolism dysregulation and ketone bodies accumulation

Succinic upregulation resembles the pseudohypoxic environment in cancer

Bruzzone et al., iScience *23*, 101645
October 23, 2020
https://doi.org/10.1016/j.isci.2020.101645

iScience

CellPress
OPEN ACCESS

Article

SARS-CoV-2 Infection Dysregulates the Metabolomic and Lipidomic Profiles of Serum

Chiara Bruzzone,[1,9] Maider Bizkarguenaga,[1,9] Rubén Gil-Redondo,[1] Tammo Diercks,[2] Eunate Arana,[3] Aitor García de Vicuña,[3] Marisa Seco,[4] Alexandre Bosch,[5] Asís Palazón,[5] Itxaso San Juan,[1] Ana Laín,[1] Jon Gil-Martínez,[1] Ganeko Bernardo-Seisdedos,[6] David Fernández-Ramos,[1,7] Fernando Lopitz-Otsoa,[1] Nieves Embade,[1] Shelly Lu,[8] José M. Mato,[1] and Oscar Millet[1,6,10,*]

SUMMARY

COVID-19 is a systemic infection that exerts significant impact on the metabolism. Yet, there is little information on how SARS-CoV-2 affects metabolism. Using NMR spectroscopy, we measured the metabolomic and lipidomic serum profile from 263 (training cohort) + 135 (validation cohort) symptomatic patients hospitalized after positive PCR testing for SARS-CoV-2 infection. We also established the profiles of 280 persons collected before the coronavirus pandemic started. Principal-component analysis discriminated both cohorts, highlighting the impact that the infection has on overall metabolism. The lipidomic analysis unraveled a pathogenic redistribution of the lipoprotein particle size and composition to increase the atherosclerotic risk. In turn, metabolomic analysis reveals abnormally high levels of ketone bodies (acetoacetic acid, 3-hydroxybutyric acid, and acetone) and 2-hydroxybutyric acid, a readout of hepatic glutathione synthesis and marker of oxidative stress. Our results are consistent with a model in which SARS-CoV-2 infection induces liver damage associated with dyslipidemia and oxidative stress.

INTRODUCTION

SARS-CoV-2 is a highly transmissible virus described for the first time in Wuhan (Hubei Province, China) in December 2019 (Zhu et al., 2020). Yet, there are evidences showing that SARS-CoV-2 emerged in Europe earlier than thought, after the analysis of wastewater samples collected in Italy by December 2019 (La Rosa et al., 2020) The virus shares sequence identity with other related coronaviruses such as SARS-CoV and MERS-CoV (Zhou et al., 2020b). Upon viral infection, an incubation period ranging from 1 to 14 days (Lauer et al., 2020) results in the onset of COVID-19 disease (Munster et al., 2020). Unfortunately, this mechanism is very efficient and SARS-CoV-2 has rapidly spread worldwide, resulting in the ongoing coronavirus pandemic. According to the World Health Organization, more than 26 million cases have been reported worldwide, having thus far resulted in about 864.000 deaths (WHO, 2020).

There are a plethora of symptoms associated to COVID-19 including fever, non-productive cough, tiredness, sore throat, nasal congestion, diarrhea, conjunctivitis, headache, dyspnea, nausea/vomiting, and in some cases loss of taste, loss of smell, or skin problems (Song et al., 2020; Tammaro et al., 2020; Wei et al., 2020). In many cases the prognosis is favorable, but approximately 20% COVID-19 patients require intensive care unit admission due to severe acute respiratory syndrome, which may be accompanied by multiorgan failure (Richardson et al., 2020). Such patients also may develop neurological problems (Niazkar et al., 2020) or hematological abnormalities (Liu et al., 2020) and suffer venous thromboembolism (Al-Ani et al., 2020). The mortality rate is very high (ca. 17%) among the elderly or people with chronic diseases (Zhou et al., 2020a).

The disease etiology is progressively being unraveled, but the underlying molecular mechanisms and the associated metabolic alterations remain much more poorly understood. To the best of our knowledge, there are only three public studies that analyzed the metabolism of patients with COVID-19 (Shen et al., 2020; Thomas et al., 2020; Wu et al., 2020). The observed molecular changes in the sera of COVID-19 patients implied significant metabolic suppression as well as a dysregulation of the macrophage function,

[1]Precision Medicine and Metabolism Laboratory, CIC bioGUNE, Basque Research and Technology Alliance, 48160 Derio, Spain

[2]NMR Platform, CIC bioGUNE, Basque Research and Technology Alliance, 48160 Derio, Spain

[3]Biocruces Bizkaia Health Research Institute, Cruces University Hospital, Osakidetza, 48903 Barakaldo, Spain

[4]OSARTEN Kooperativa Elkartea, 20500 Arrasate-Mondragón, Spain

[5]Cancer Immunology and Immunotherapy Lab, CIC bioGUNE, Basque Research and Technology Alliance, 48160 Derio, Spain

[6]ATLAS Molecular Pharma S. L., 48160 Derio, Spain

[7]CIBERehd, Instituto de Salud Carlos III Madrid, Spain

[8]Division of Digestive and Liver Diseases, Department of Medicine, Cedars-Sinai Medical Center, Los Angeles, CA 90048, US

[9]These authors contributed equally

[10]Lead Contact

*Correspondence: omillet@cicbiogune.es

https://doi.org/10.1016/j.isci.2020.101645

platelet degranulation, and the complement system pathway among others. These results are in line with the mechanism observed for other viral infections like Ebola (Kyle et al., 2019) and highlight the systemic characteristic of the disease that may affect further organs such as the liver. Yet, these conclusions were mostly obtained from proteomics data and would demand complementary metabolomic analyses of much larger cohorts.

The aim of this study was to investigate whether there is a specific metabolic and/or lipoprotein profile associated with patients diagnosed with COVID-19 by a positive RT-PCR testing and showing clear manifestations of the disease. To that end, we have used NMR-based metabolomics that is particularly well suited for the characterization of complex solutions like serum and is capable at the same time to quantify and identify both, known and unknown metabolites. Mass spectrometry is also widely used for metabolomics studies, because of its extreme sensitivity and ability to analyze a massive number of metabolites using very small sample amounts. That said, NMR is fully quantitative and can also classify and quantify lipoproteins in a robust and reliable way, with higher resolution than ultracentrifugation (Chapman et al., 1981). We have analyzed a cohort with 263 COVID-19-positive serum samples obtained from patients hospitalized after positive PCR testing for SARS-CoV-2 infection (information about the patients is shown in Tables S2 and S3). As a control, we have analyzed the sera from 280 persons collected during 2018–2019, well before the coronavirus pandemic started. Our results show that COVID-19 patients present a severe metabolic and lipoprotein dysregulation, compatible with induced dyslipidemia and oxidative stress among other metabolic factors.

RESULTS

SARS-CoV-2 Infection Significantly Rewires the Metabolome and the Lipoprotein Composition

To investigate the metabolic and lipidomic changes induced by SARS-CoV-2 infection, we analyzed a cohort of 263 COVID-19 patients by NMR spectroscopy (*COVID*). These individuals presented compatible symptomatology that was confirmed by PCR testing upon admission to the hospital. A subset of 43 samples from the *COVID* cohort was tested for antibodies, where 21 (48%) were positive for IgG only and 11 (26%) for IgG and IgM. This sub-cohort well represents the *COVID* cohort in terms of gender and age. Hence, this set of hospitalized individuals represents well the acute and severe symptomatic phases of the disease. As a control, we employed a cohort of sera from 280 individuals of the working population from the same geographical region, but collected in pre-COVID times (2018–2019) during a routine medical check-up and with no other exclusion criteria than having suffered a serious illness like cancer or stroke within the three months preceding the sample collection (*preCOVID*).

The NMR Carr-Purcell-Meiboom-Gill spectrum (Embade et al., 2016) filters out the lipoprotein fraction, rendering the metabolic profiling of the serum. Already a visual inspection of such spectra revealed substantial differences, a notion that was further substantiated by an unsupervised principal-component analysis (PCA) of the 40 metabolites that can be routinely quantified from this type of spectrum (Figures 2A and 2B). In turn, a regular ^{1}H NMR spectrum of serum also reveals the complex lipoprotein profile (Jiménez et al., 2018), as shown in Figure 1 for representative examples of the *COVID* and *preCOVID* cohorts, where 21 main lipoprotein fractions, 74 lipoprotein subfractions, and other important serum parameters can nowadays be identified and quantified by spectra deconvolution. Such set includes lipoproteins and their respective subfractions (Table S5). The NMR spectrum also allows a detailed characterization of the different lipoprotein subclasses, with the quantification of the total and free cholesterol, phospholipids, triglycerides, Apo-A1, Apo-A2, and Apo-B. PCA shows a reasonable separation between *COVID* and *preCOVID* cohorts (Figures 2C and 2D), suggesting that SARS-CoV-2 infection may also inflict changes in the blood lipoprotein composition.

These differences observed by unsupervised analysis were also confirmed by orthogonal partial least-squares discriminant analysis (OPLS-DA) for the full set of serum metabolites and lipoprotein subclasses (Figure 2E), using one predictive and one orthogonal component. Not surprisingly, OPLS-DA showed a high degree of separation between groups, also with very good predictability ($AUROC_{validation}$ = 0.977) (Table 1) and statistical significance (p value < 0.01) (Figures S4 and S5). Remarkably, even when metabolites and all the different lipid fractions were included as independent classes in an OPLS-DA, a reasonable degree of clustering was achieved (Figure 2F).

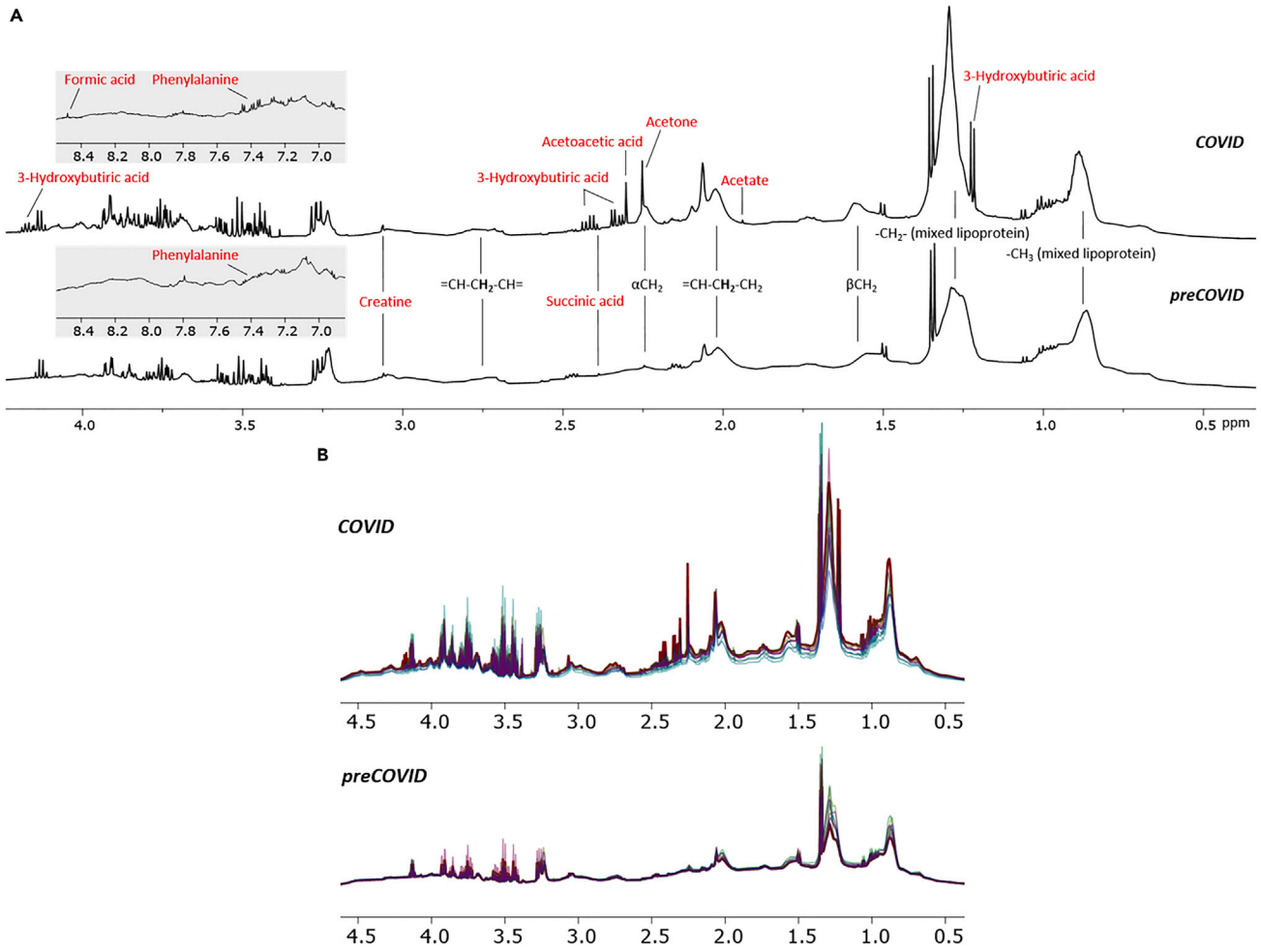

Figure 1. Representative Region of ^{1}H NMR Spectra of *COVID* and *preCOVID* Sera

(A) Metabolite identification in sera spectrum from *COVID* positive and *preCOVID*. For instance, notice the increased amount of ketone bodies (3-hydroxybutiric acid, acetoacetic acid, acetone) in the *COVID*-positive spectrum when compared with the *preCOVID* one.

(B) Overlapped nuclear Overhauser effect spectra from *COVID*-positive and *preCOVID* serum samples.

As COVID-19 severity increases particularly for elderly people, a potential caveat is the substantial age difference between the *COVID* and the *preCOVID* cohorts. Yet, two sub-cohorts of 112 samples each, properly balanced for gender and age distribution, showed the same qualitative separation for metabolites and lipoproteins in both, PCA and OPLS-DA (Figures S1 and S5, Table S4). These results rule out a bias due to improper randomization of the control group.

Another concern is that, during the peak of the pandemic, collecting protocols could not be completely abided, what could affect the results. However, the analysis of a second patient cohort from a different hospital yielded the same results (Figure S2), which strongly suggests that technical handling aspects may not decisively affect the outcome. Remarkably, the added cohort includes almost 400 patient samples, which, to our knowledge, is the largest metabolomic analysis reported in COVID-19.

The pre-COVID cohort belongs to a collection of samples from healthy population that were collected in a period of 2 years before COVID-19 outbreak. To evaluate the effect of storage of the samples, we performed a PCA of a subset of the first samples collected (in 2016), compared with the last samples to be frozen (in 2018). As shown in Figure S3, the two groups cannot be separated, indicating that the freezing period does not significantly bias the cohort.

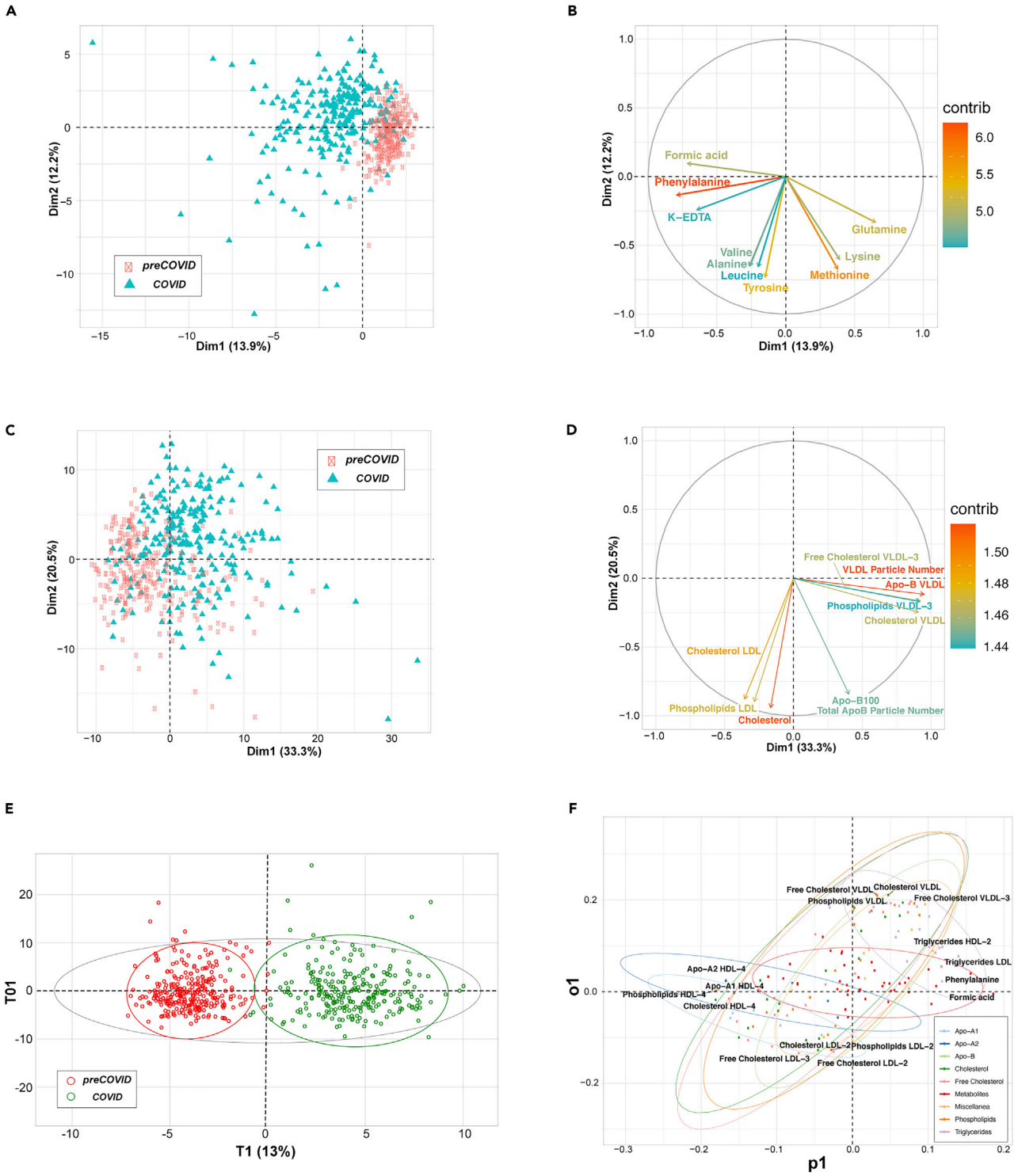

Figure 2. Summary of Multivariate Unsupervised (PCA) and Supervised (OPLS-DA) Analyses

(A and C) Score plots representing first two principal components from PCA of serum metabolites (A) and lipoprotein subclasses (C), colored by cohort. Each axis indicates the percentage of total variability explained by the component.

(B and D) Loading plots from serum metabolites PCA (B) and lipoprotein subclasses PCA (D). They show the top 10 variables with the highest contribution to the first two PCA components. Their direction indicates how their weight is distributed in both components, and the color is the percentage of contribution.

Figure 2. *Continued*

(E) Score plot from OPLS-DA between *COVID* (green) and *preCOVID* (red) cohorts, using the full list of metabolites and lipoprotein subclasses. The plot shows the main component versus the first orthogonal component.

(F) Loading plot from the previous OPLS-DA. Each type of variable (metabolites or the lipoprotein subclasses) is represented with different colors. For each type, ellipses surround the area that includes 95% of their members. For each direction, the four variables that most contribute to the component are labeled.

Lipoprotein Profiling Unravels Increased Atherogenic Risk in COVID-19 Patients

It is instructive to analyze the changes observed upon SARS-CoV-2 infection in more depth because it is already known that SARS-CoV-2, SARS-CoV-1, or MERS-CoV infection may affect the liver (Kukla et al., 2020), eventually inducing long-term injury in some patients (Wu et al., 2017). The effect of SARS-CoV-2 infection on the different lipoprotein classes and subclasses, as analyzed by ^{1}H NMR, is summarized in Figures 2D and 3 and Table S1. Our findings are consistent with a triglyceride (TG)-rich lipoprotein profile in the *COVID* cohort: serum TG content and the mean concentration of TG-VLDL (VLDL, very low density lipoproteins), TG-IDL (IDL, intermediate density lipoproteins), TG-LDL (LDL, low density lipoproteins), and TG-HDL (HDL, high density lipoproteins) were significantly increased in COVID-19 patients. Among these, the largest increase (by factor 2) was observed for TG-LDL (Figure 3). Inversely, the total cholesterol (TC) and mean concentration of bound TC-LDL and TC-HDL (both are the main carriers of cholesterol) were decreased in COVID-19 serum, most prominently for TC-HDL subfractions 4 and 3. In contrast, TC-VLDL and TC-IDL levels were slightly, but significantly, increased. The concentrations of cholesteryl esters and phospholipids in the main lipoprotein classes showed a profile similar to that observed for TG and TC. All these observations suggest a remodeling of the lipoprotein particle phenotype in COVID-19 patients, with a reduction of the mean HDL size, an enlargement of the mean size of LDL, and increased level of VLDL subclasses with intermediate size.

Among the apolipoproteins, both Apo-A1 and Apo-A2, the major apoprotein components of HDL, markedly decreased in COVID-19 patient serum, although they maintained a normal Apo-A1 to Apo-A2 ratio, indicating that SARS-CoV-2 infection did not alter HDL composition. The Apo-B to Apo-A1 ratio, a balance between atherogenic and anti-atherogenic particles, markedly increased by about 2-fold indicating an increased cardiovascular risk for COVID-19 patients.

Low-Molecular-Weight Metabolite Profiling Shows Indications of Liver Damage in COVID-19 Patients

Our analysis of low-molecular-mass metabolites NMR showed that ketone bodies (acetoacetic acid, 3-hydroxybutyric acid, and acetone) were markedly elevated in the serum of COVID-19 patients. Acetoacetic acid increased from 1.14×10^{-2} to 5.54×10^{-2} mmol/L ($p < 0.0001$, 385%), 3-hydroxybutyric acid from 6.6×10^{-2} to 2.7×10^{-1} mmol/L ($p < 0.0001$, 302%), and acetone from 2.75×10^{-2} to 6.45×10^{-2} mmol/L ($p < 0.0001$, 134%) (Figure 4). It is known that ketone bodies are induced by fasting conditions (Scott and Deuster, 2017), but we observed elevated ketone bodies for the patient's cohort (collected under uncontrolled fasting conditions) when compared with the pre-COVID cohort (collected under fasting conditions). Therefore, the differences shown in the amount of ketone bodies can be only attributed to the disease. Moreover, recent medical reports also suggest that COVID-19 implies ketone bodies accumulation (Li et al., 2020). As ketone bodies are produced predominantly in the liver from fatty acid oxidation-derived acetyl-CoA, the observed serum accumulation of TG and TG-VLDL in COVID-19 patients, shown in Figure 3, may be due to a reduced hepatic capacity to oxidize acetyl-CoA in the mitochondria, which is then redirected to the synthesis of acetoacetic acid and 2-hydroxybutyric acid. The elevation of glucose in the serum of COVID-19 patients (8.19 versus 4.89 mmol/L, $p < 0.0001$, 68%) (Figure 4) is consistent with this model, because mitochondrial oxaloacetate is driven to the cytoplasm into gluconeogenesis, via the synthesis of malic acid, when it cannot condensate with acetyl-CoA to feed the tricarboxylic acid cycle. The increase in succinic acid, citric acid, glutamic acid, and pyruvic acid by 156%, 12%, 33%, and 67%, respectively (Figure 4), may all be related to this dysregulation of hepatic central carbon metabolism in COVID-19 patients. In addition to the metabolic re-wiring that may result as a consequence of central carbon metabolism dysregulation, the accumulation of succinic acid has been shown to create a pseudohypoxic environment that facilitates cancer development and progression (Klukova et al., 2018). Moreover, the reduction in the essential amino acids methionine, isoleucine, histidine, and lysine by 19%, 11%, 16%, and 34%, respectively, together with the reduction of tyrosine and glutamine by 4%, and 19%, respectively, two amino acids whose synthesis can be limited under special pathophysiological conditions, along with

Metric	Training		Validation	
	Value	p Value	*Value*	p Value
AUROC	0.980	<0.01	0.977	<0.01
Accuracy	0.928	<0.01	0.923	<0.01
Sensitivity	0.874	<0.01	0.867	<0.01
Specificity	0.978	<0.01	0.975	<0.01

Table 1. Performance Metrics from OPLS-DA through a Repeated Double Cross-Validation Process
Value columns are the mean value; p value columns were obtained from permutation tests.

substantially increased levels of phenylalanine (an essential amino acid precursor of tyrosine) and 2-hydroxybutiryc acid (a readout of hepatic oxidative stress), which increased by 81%, and 628%, respectively (Figure 4), altogether suggests the existence of a general metabolic stress condition in COVID-19 patients.

DISCUSSION

We have here investigated the changes that SARS-CoV-2 infection may provoke in the metabolism, by measuring the serum concentrations of various lipoproteins and metabolites using ^{1}H NMR spectroscopy. To that end we have investigated a large cohort of patients (n = 263) at the moment of hospitalization, all with COVID-19-compatible symptomatology and 100% of them confirmed by RT-PCR testing. From the antibody test, 75% of the patients also already developed IgG antibodies, and about a third of them, also IgM antibodies. Importantly, these patients did not necessarily have previous health problems as the only inclusion criterion was the SARS-CoV-2 infection. Taken together, this patient cohort is, on average, representing the acute symptomatic phase of the disease, approximately between 14 and 21 days from onset. As a control cohort, we have used a pool of samples of similar size (n = 280), that belongs to healthy population and acquired before the advent of COVID-19. Although the two cohorts have different average age, we have demonstrated that this is not a contributing factor to the observed differences (Figure S1).

One of the most striking differences arises from the lipoprotein distribution. Endogenous lipoproteins are classified according to lipid and apolipoprotein composition in VLDL, IDL, LDL, and HDL (Feingold KR, 2018). HDL is classified as atheroprotective because it is involved in the transport of cholesterol to the liver. Upon an excess of fatty acids and TC in the liver, these lipids are converted into TG and cholesteryl esters, respectively; wrapped with apolipoproteins (mainly Apo-B), decorated with phospholipids; and placed into circulation as VLDL where, via capillaries, they get in contact with the various tissues. Our NMR analysis clearly reflects a scenario with a severe lipoprotein dysregulation toward increased TG and abnormal lipoprotein particle distribution, with an increase of VLDL subclasses with intermediate size. These results are in line with other observations using MS (Shen et al., 2020; Thomas et al., 2020), but our study, on a very large cohort, adds granularity to the lipoprotein distribution and allows devising a detailed landscape of lipoprotein rearrangement upon SARS-CoV-2 infection. This acute dysregulation is obviously pathogenic, and, when found in non-acute episodes such as metabolic syndrome or non-alcoholic fatty liver disease, it would fit well with increased atherosclerotic risk.

The metabolic profile of COVID-19 patients, also obtained by NMR spectroscopy, agrees well with the lipidomic analysis. The excess of ketone bodies (acetone, acetoacetic acid, and 3-hydroxybutyric acid) suggests that they are being used as an alternative energy source due to a sort of diabetic ketoacidosis. Consistently, glucose levels are also elevated, but this has to be taken with extreme caution because samples were not collected at fasting conditions. Some other metabolites such as succinate and pyruvate among others are consistent with impaired central metabolism and/or mitochondrial dysfunction. We have recently observed that thrombocytopenia in COVID-19 patients (Connors and Levy, 2020) ultimately results in elevated porphyrin levels, in a similar way as observed in porphyria, a family of diseases that always imply oxidative stress, mitochondrial impairment, and liver damage.

Furthermore, the analysis of low-molecular-weight metabolites reveals the presence of general metabolic stress in COVID-19 patients, as indicated by the increase in 2-hydroxybutiryc acid (hepatic oxidative stress

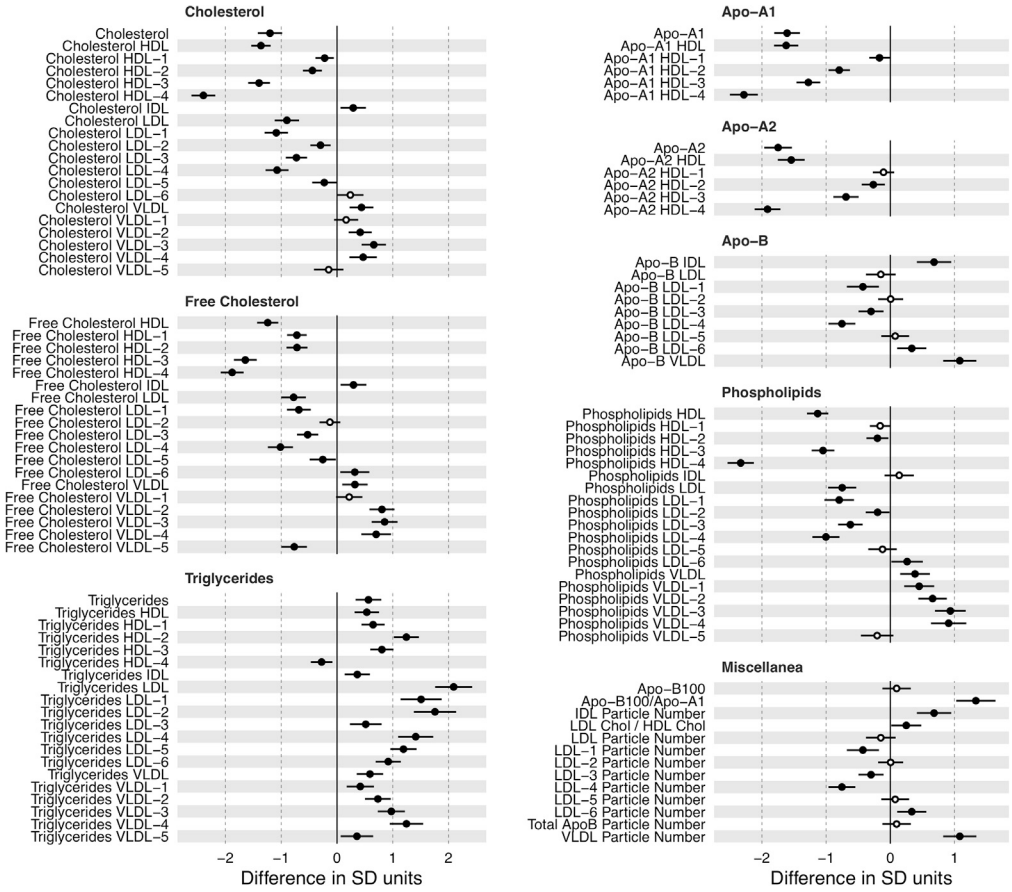

Figure 3. Average Effect of COVID-19 for Each Lipoprotein Subclass

Horizontal axis is the number of standard deviations that a variable is on average increased (or decreased) when an individual is positive for COVID-19. Circles are positioned in the specific mean increase (decrease) value, whereas horizontal black bars are the 95% confidence interval. Statistically significant differences (p value < 0.05) are represented with filled circles.

marker), and the reduction in essential amino acids, tyrosine, and glutamine. In summary, herein we provide an observational report of the comprehensive serum metabolome of a very large cohort of COVID-19-positive patients in the acute phase of the disease. Our results evidence massive changes in the lipoprotein and metabolomic profiles consistent with the observed blood alterations in COVID-19 patients, highlighting the systemic character of the disease.

Limitations of the Study

The cohort is limited to the same world region, which may partially compromise the generality of the conclusions due to geographical biases. Freezing the samples may alter the metabolite concentrations, even though the two control groups (Figure S3) suggest that this problem does not significantly affect the conclusions of the present study. Samples that were collected before the pandemic (*pre*COVID) may have not used the same protocol as the COVID cohorts. All the samples correspond to the acute phase of the disease, and the study would benefit from the study of samples from patients at different stages of the SARS-CoV-2 infection.

Resource Availability

Lead Contact

Further information and requests for resources and reagents should be directed to and will be fulfilled by the Lead Contact, Oscar Millet (omillet@cicbiogune.es).

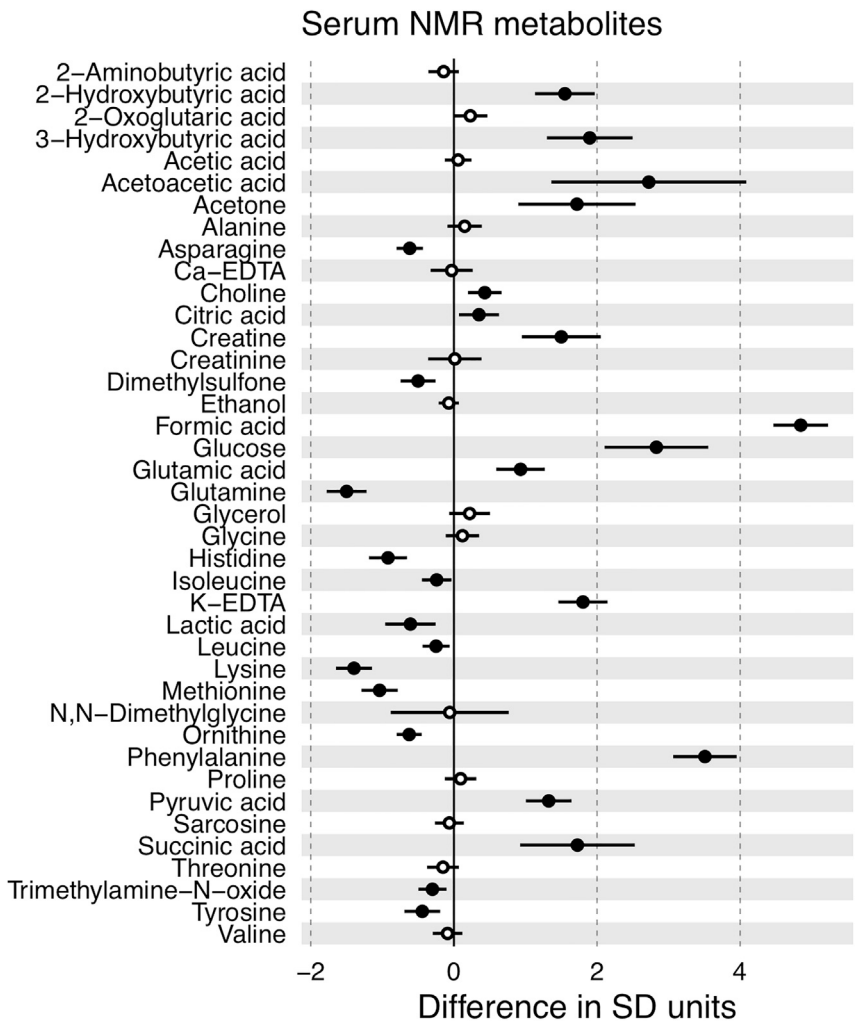

Figure 4. Average Effect of COVID-19 for Each Metabolite

Horizontal axis is the number of standard deviations that a variable is on average increased (or decreased) when an individual is positive for COVID-19. Circles are positioned in the specific mean increase (decrease) value, whereas horizontal black bars are the 95% confidence interval. Statistically significant differences (p value < 0.05) are represented with filled circles.

Materials Availability

This study did not generate new unique reagents.

Data and Code Availability

All parameter values, datasets, and used in the model are included in the Supplemental Information.

METHODS

All methods can be found in the accompanying Transparent Methods supplemental file.

SUPPLEMENTAL INFORMATION

Supplemental Information can be found online at https://doi.org/10.1016/j.isci.2020.101645.

ACKNOWLEDGMENTS

Support was provided by the Department of Economic Development and Infrastructures of the Government of the Autonomous Community of the Basque Country (Elkartek BG2019) and the Severo Ochoa

Excellence Accreditation from MCIU (SEV-2016-0644). O.M. acknowledges the Agencia Estatal de Investigación (Spain) for grants CTQ2015-68756-R, RTI2018-101269-B-I00. J.M.M. acknowledges the Agencia Estatal de Investigación (Spain) and CIBERehd for grants SAF2017-88041-R. O.M. and J.M.M. acknowledge NIH 1R01DK119437-01A1.

AUTHOR CONTRIBUTIONS

E.A., M.S., and A.G.d.V. collected the samples; I.S.J., C.B., M.B., G.B.-S., A.L., P.U., J.G.-M., and T.D. performed the experiments; R.G.-R. and N.E. performed the statistical data analysis; J.M.M. and O.M. designed research, and O.M. wrote the paper.

DECLARATION OF INTEREST

The authors declare no competing interests.

Received: July 1, 2020
Revised: September 22, 2020
Accepted: September 30, 2020
Published: October 23, 2020

REFERENCES

Al-Ani, F., Chehade, S., and Lazo-Langner, A. (2020). Thrombosis risk associated with COVID-19 infection. A scoping review. Thromb. Res. *192*, 152–160.

Connors, J.M., and Levy, J.H. (2020). COVID-19 and its implications for thrombosis and anticoagulation. Blood *135*, 2033–2040.

Chapman, M.J., Goldstein, S., Lagrange, D., and Laplaud, P.M. (1981). A density gradient ultracentrifugal procedure for the isolation of the major lipoprotein classes from human serum. J. Lipid Res. *22*, 339–358.

Embade, N., Mariño, Z., Diercks, T., Cano, A., Lens, S., Cabrera, D., Navasa, M., Falcón-Pérez, J.M., Caballería, J., Castro, A., et al. (2016). Metabolic characterization of advanced liver fibrosis in HCV patients as studied by serum 1H-NMR spectroscopy. PLoS One *11*, e0155094.

Feingold KR, G.C. (2018). Introduction to Lipids and Lipoproteins (MDText.com, Inc).

Jiménez, B., Holmes, E., Heude, C., Tolson, R.F., Harvey, N., Lodge, S.L., Chetwynd, A.J., Cannet, C., Fang, F., Pearce, J.T.M., et al. (2018). Quantitative lipoprotein subclass and low molecular weight metabolite analysis in human serum and plasma by (1)H NMR spectroscopy in a multilaboratory trial. Anal. Chem. *90*, 11962–11971.

Klukova, K., and Tennant, D. (2018). Metabolic implications of hypoxia and pseudohypoxia in pheochromocytoma and paraganglioma. Cell Tissue Res. *372*, 367–378.

Kukla, M., Skonieczna-Żydecka, K., Kotfis, K., Maciejewska, D., Łoniewski, I., Lara, L.F., Pazgan-Simon, M., Stachowska, E., Kaczmarczyk, M., Koulaouzidis, A., et al. (2020). COVID-19, MERS and SARS with concomitant liver injury-systematic review of the existing literature. J. Clin. Med. *9*, 1420.

Kyle, J.E., Burnum-Johnson, K.E., Wendler, J.P., Eisfeld, A.J., Halfmann, P.J., Watanabe, T., Sahr, F., Smith, R.D., Kawaoka, Y., Waters, K.M., et al. (2019). Plasma lipidome reveals critical illness and recovery from human Ebola virus disease. Proc. Natl. Acad. Sci. U S A *116*, 3919–3928.

La Rosa, G., Mancini, P., Bonanno Ferraro, G., Veneri, C., Iaconelli, M., Bonadonna, L., Lucentini, L., and Suffredini, E. (2020). SARS-CoV-2 has been circulating in northern Italy since December 2019: evidence from environmental monitoring. Sci. total Environ. *750*, 141711.

Lauer, S.A., Grantz, K.H., Bi, Q., Jones, F.K., Zheng, Q., Meredith, H.R., Azman, A.S., Reich, N.G., and Lessler, J. (2020). The incubation period of coronavirus disease 2019 (COVID-19) from publicly reported confirmed cases: estimation and application. Ann. Intern. Med. *172*, 577–582.

Li, J., Wang, X., Chen, J., Zuo, X., Zhang, H., and Deng, A. (2020). COVID-19 infection may cause ketosis and ketoacidosis. Diabetes Obes. Metab. https://doi.org/10.1111/dom.14057.

Liu, X., Zhang, R., and He, G. (2020). Hematological findings in coronavirus disease 2019: indications of progression of disease. Ann. Hematol. 1–8.

Munster, V.J., Koopmans, M., van Doremalen, N., van Riel, D., and de Wit, E. (2020). A novel coronavirus emerging in China - key questions for impact assessment. New Engl. J. Med. *382*, 692–694.

Niazkar, H.R., Zibaee, B., Nasimi, A., and Bahri, N. (2020). The neurological manifestations of COVID-19: a review article. Neurol. Sci. *41*, 1667–1671.

Richardson, S., Hirsch, J.S., Narasimhan, M., Crawford, J.M., McGinn, T., Davidson, K.W., Barnaby, D.P., Becker, L.B., Chelico, J.D., Cohen, S.L., et al. (2020). Presenting characteristics, comorbidities, and outcomes among 5700 patients hospitalized with COVID-19 in the New York city area. Jama *323*, 2052–2059.

Scott, J.M., and Deuster, P.A. (2017). Ketones and human performance. J. Spec. operations Med. *17*, 112–116.

Shen, B., Yi, X., Sun, Y., Bi, X., Du, J., Zhang, C., Quan, S., Zhang, F., Sun, R., Qian, L., et al. (2020). Proteomic and metabolomic characterization of COVID-19 patient sera. Cell *S0092-8674*, 30627–30629.

Song, Y., Liu, P., Shi, X.L., Chu, Y.L., Zhang, J., Xia, J., Gao, X.Z., Qu, T., and Wang, M.Y. (2020). SARS-CoV-2 induced diarrhoea as onset symptom in patient with COVID-19. Gut *69*, 1143–1144.

Tammaro, A., Adebanjo, G.A.R., Parisella, F.R., Pezzuto, A., and Rello, J. (2020). Cutaneous manifestations in COVID-19: the experiences of barcelona and Rome. J. Eur. Acad. Dermatol. Venereol. *34*, e306–e307.

Thomas, T., Stefanoni, D., Reisz, J.A., Nemkov, T., Bertolone, L., Francis, R.O., Hudson, K.E., Zimring, J.C., Hansen, K.C., Hod, E.A., et al. (2020). COVID-19 infection results in alterations of the kynurenine pathway and fatty acid metabolism that correlate with IL-6 levels and renal status. medRxiv. https://doi.org/10.1101/2020.05.14.20102491.

Wei, X.S., Wang, X., Niu, Y.R., Ye, L.L., Peng, W.B., Wang, Z.H., Yang, W.B., Yang, B.H., Zhang, J.C., Ma, W.L., et al. (2020). Diarrhea is associated with prolonged symptoms and viral carriage in corona virus disease 2019. Clin. Gastroenterol. Hepatol. *18*, 1753–1759.e2.

WHO. www.who.int/emergencies/diseases/novel-coronavirus-2019/situation-reports/.

Wu, D., Shu, T., Yang, X., Song, J.-X., Zhang, M., Yao, C., Liu, W., Huang, M., Yu, Y., Yang, Q., et al. (2020). Plasma metabolomic and lipidomic alterations associated with COVID-19. Natl. Sci. Rev. nwaa086.

Wu, Q., Zhou, L., Sun, X., Yan, Z., Hu, C., Wu, J., Xu, L., Li, X., Liu, H., Yin, P., et al. (2017). Altered lipid metabolism in recovered SARS patients twelve years after infection. Sci. Rep. *7*, 9110.

Zhou, F., Yu, T., Du, R., Fan, G., Liu, Y., Liu, Z., Xiang, J., Wang, Y., Song, B., Gu, X., et al. (2020a). Clinical course and risk factors for mortality of adult inpatients with COVID-19 in Wuhan, China: a retrospective cohort study. Lancet (London, England) *395*, 1054–1062.

Zhou, P., Yang, X.-L., Wang, X.-G., Hu, B., Zhang, L., Zhang, W., Si, H.-R., Zhu, Y., Li, B., Huang, C.-L., et al. (2020b). Discovery of a novel coronavirus associated with the recent pneumonia outbreak in humans and its potential bat origin. bioRxiv. https://doi.org/10.1038/s41586-020-2012-7.

Zhu, N., Zhang, D., Wang, W., Li, X., Yang, B., Song, J., Zhao, X., Huang, B., Shi, W., Lu, R., et al. (2020). A novel coronavirus from patients with pneumonia in China, 2019. N. Engl. J. Med. *382*, 727–733.

iScience, Volume *23*

Supplemental Information

SARS-CoV-2 Infection Dysregulates the Metabolomic and Lipidomic Profiles of Serum

Chiara Bruzzone, Maider Bizkarguenaga, Rubén Gil-Redondo, Tammo Diercks, Eunate Arana, Aitor García de Vicuña, Marisa Seco, Alexandre Bosch, Asís Palazón, Itxaso San Juan, Ana Laín, Jon Gil-Martínez, Ganeko Bernardo-Seisdedos, David Fernández-Ramos, Fernando Lopitz-Otsoa, Nieves Embade, Shelly Lu, José M. Mato, and Oscar Millet

Supplemental Information

Supplemental Figures

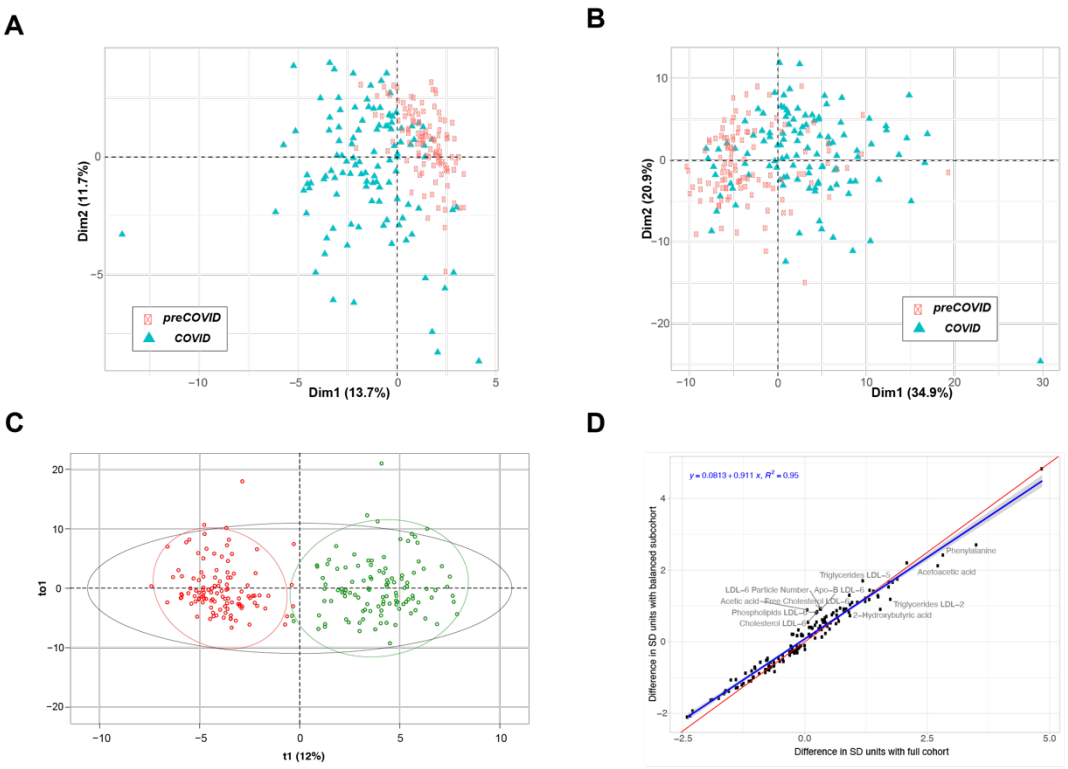

Figure S1. Analysis of balanced sub-cohorts and their comparison to full cohorts, Related to Figure 1. A-B) Score plots, from multivariate unsupervised (PCA), representing first two principal components from PCA of serum metabolites (A) and lipoprotein subclasses (B), colored by sub-cohort. Each axis indicates the percentage of total variability explained by the component. (C) Score plot from OPLS-DA between *COVID* (green) and *preCOVID* (red) sub-cohorts using the full list of metabolites and lipoprotein subclasses. The plot shows the main component vs. the first orthogonal component. (D) Comparison of effect of COVID-19 over the different metabolites/protein subclasses analyzed with full cohorts and with balanced sub-cohorts. Blue line is the linear model between both analyses, while red line is the identity. Those samples with an absolute difference bigger than 0.5 between both analyses are labeled.

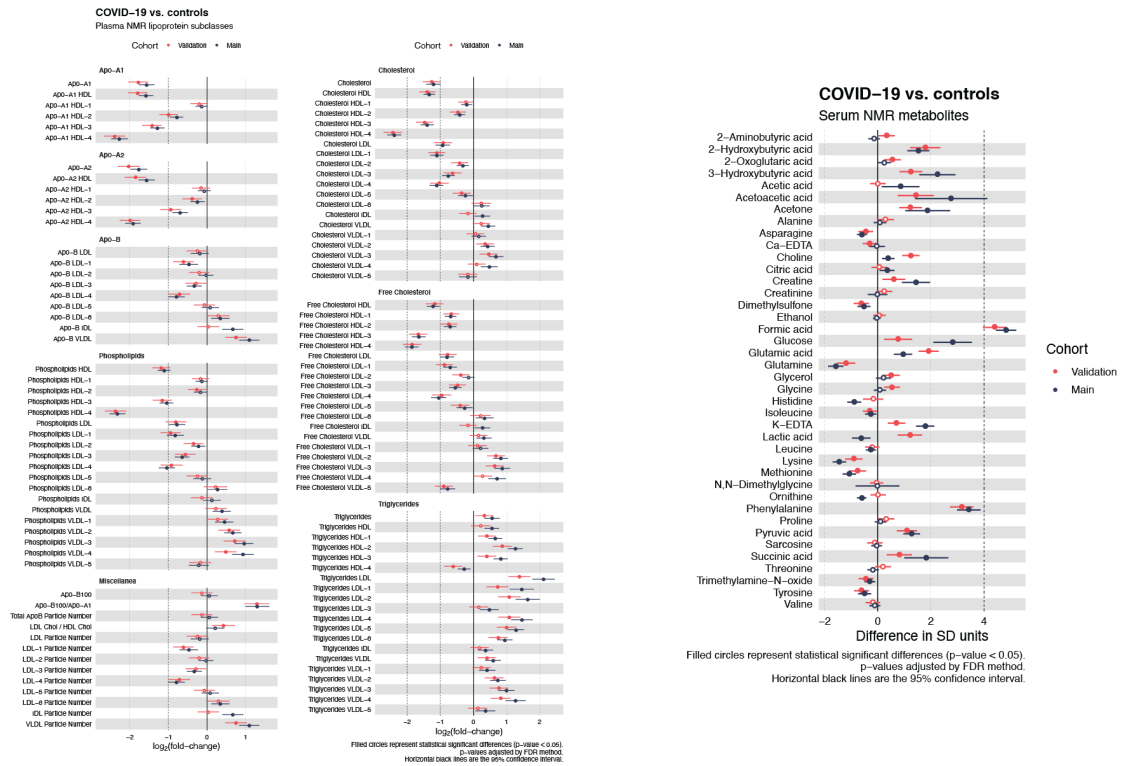

Figure S2. Validation cohort analysis, Related to Figures 3 and 4. Average effect of COVID-19 for each lipoprotein subclass and metabolite in both patient cohorts against preCOVID cohort. Main cohort represent samples from the first hospital and Validation cohort represent samples from the second hospital. Horizontal axis is the number of standard deviations that a variable is on average increased (or decreased) when an individual is positive in COVID-19. Circles are positioned in the specific mean increase (decrease) value, while horizontal black bars are the 95% confidence interval. Statistically significant differences (p-value < 0.05) are represented with filled circles.

Figure S3. PCA for two subset of control samples with a difference in 400 days of freezing period, Related to Figure 1.

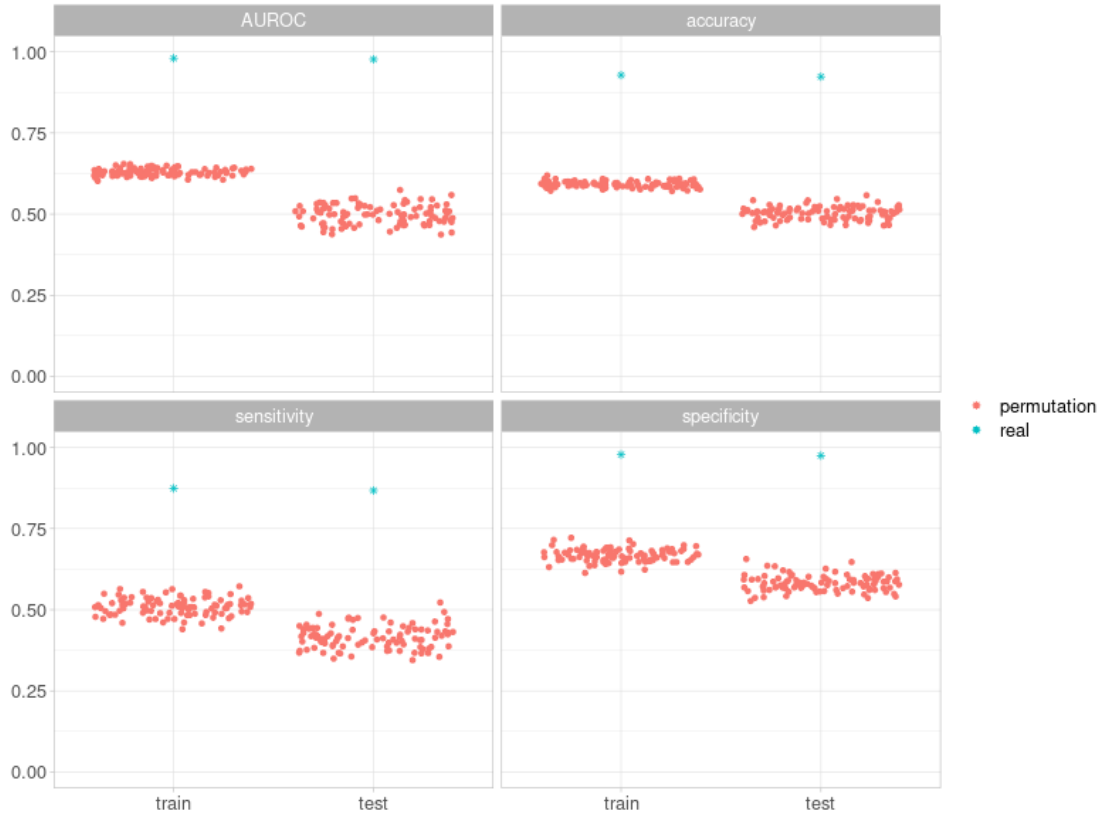

Figure S4. Permutation test for the main cohort, Related to Figure 1. Results of 100 permutation tests compared to real values for each metric obtained from repeated double cross validation.

Figure S5. Permutation test for the balanced subcohort, Related to Figure 1. Results of 100 permutation tests compared to real values for each metric obtained from repeated double cross validation in balanced subcohort.

Supplemental Tables

Table S1. Concentrations of metabolites and lipoproteins, Related to Figures 3 and 4. The Table has been deposited in Mendeley Data:

Millet, Oscar (2020), "SARS-CoV-2 infection dysregulates the metabolomic and lipidomic profiles of serum. Bruzzone et al.", Mendeley Data, V1, doi: 10.17632/3h96n97xrb.1

Table S2. Metadata from the Individuals Analyzed. Related to Figures 1-4.

	preCOVID ***N=280***	**COVID** ***N=263***	**p-value**	**N**
Main info				
Gender (female)	146 (52.14%)	116 (45.14%)	0.124	537
Age (years)	48.89±11.00	64.81±16.64	<0.001	537
Total hospitalization days	-	13.72±19.60	-	257
Days in ICU	-	5.12±16.52	-	257
Smoker	45 (16.07%)	17 (6.61%)	0.001	537
Pneumonia:			-	248
unilateral	-	33 (13.31%)	-	
bilateral	-	173 (69.76%)	-	
Death	-	24 (9.34%)	-	257
Signs at admission				
Temperature (ºC)	-	36.47±0.91	-	249
Breathing freq. (n x min.)	-	22.29±7.98	-	65
Heart rate (n x min.)	-	90.82±17.36	-	250
Systolic blood pressure (mm Hg)	-	135.72±23.08	-	250
Diastolic blood pressure (mm Hg)	-	78.24±12.73	-	251
Commorbidities				
Cardiovascular	-	68 (26.46%)	-	257
Cerebrovascular	-	18 (7.00%)	-	257
Diabetes	18 (6.43%)	64 (24.90%)	<0.001	537
EPOC	-	29 (11.28%)	-	257
Hypertension	50 (18.12%)	116 (45.14%)	<0.001	533
Immunodeficiency	-	11 (4.28%)	-	257
Liver failure	-	4 (1.56%)	-	257
Neoplasm	-	31 (12.06%)	-	257
Renal insufficiency	-	21 (8.17%)	-	257
Symptoms				
Clouding of conciousness	-	20 (7.78%)	-	257
Conjunctival congestion	-	2 (0.78%)	-	257
Diarrhea	-	75 (29.18%)	-	257

Disorientation	-	11 (4.28%)	-	257
Dry cough	-	135 (52.53%)	-	257
Fatigue	-	148 (57.59%)	-	257
Fever	-	177 (68.87%)	-	257
Headache	-	49 (19.07%)	-	257
Hemoptysis	-	1 (0.39%)	-	257
Lymphadenopathy	-	3 (1.17%)	-	257
Myalgia	-	75 (29.18%)	-	257
Nasal congestion	-	11 (4.28%)	-	257
Nausea Vomiting	-	38 (14.84%)	-	256
Odynophagia	-	31 (12.06%)	-	257
Oropharyngeal congestion	-	1 (0.39%)	-	257
Productive cough	-	58 (22.57%)	-	257
Shaking chills	-	55 (21.40%)	-	257
Skin rash	-	3 (1.17%)	-	257
Blood test				
Albumin (g/dL)	-	3.69±0.42	.	136
ALT (U/L)	22.26±11.90	34.09±26.08	<0.001	528
APTT (s)	-	24.27±4.83	.	252
Bilirubin (mg/dL)	0.50±0.23	0.74±0.46	0.002	164
C-reactive protein (mg/L)	-	77.32±71.33	.	255
Creatinine (mg/dL)	0.82±0.16	1.06±0.81	<0.001	535
Creatine phosphokinase (U/L)	-	158.26±331.91	.	233
D-dimer (ng/mL)	-	2508.72±9149.53	.	248
Ferritin (ng/mL)	47.29±49.13	670.80±772.35	<0.001	254
Glucose (mg/dL)	88.26±16.07	136.09±87.94	<0.001	535
Interleukin 6 (pg/mL)	-	19.50±24.78	-	12
Lactate dehydrogenase (U/L)	-	318.70±205.66	-	247
Leukocytes (10^9/L)	6.91±1.81	7.58±5.15	0.050	534
Lymphocytes (10^9/L)	2.41±0.77	1.20±1.30	<0.001	534
Monocytes (10^9/L)	0.63±0.19	0.42±0.24	<0.001	535
Neutrophils (10^9/L)	3.59±1.37	6.02±6.02	<0.001	534
Platelets (10^9/L)	237.43±45.86	218.03±109.86	0.009	534
Procalcitonin (ng/mL)	-	0.37±0.78	-	130
Protein (g/dL)	-	6.35±0.57	-	145
Prothrombin activity (%)	-	87.85±21.82	-	234
Urea (mg/dL)	-	44.20±29.86	-	255

Table S3. Metadata from the Individuals Analyzed (balanced subcohort), Related to Figure 1.

	preCOVID ***N=112***	**COVID** ***N=112***	**p-value**	**N**
Main info				
Gender (female)	59 (52.68%)	59 (52.68%)	1.000	224

Age (years)	49.86±10.66	49.86±10.66	1.000	224
Total hospitalization days	-	8.77±13.41	-	112
Days in ICU	-	2.63±9.13	-	112
Smoker	20 (17.86%)	13 (11.61%)	0.258	224
Pneumonia:			-	109
unilateral	-	19 (17.43%)		
bilateral	-	69 (63.30%)		
Death	-	2 (1.79%)	-	112
Signs at admission				
Temperature (ºC)	-	36.42±0.74	-	109
Breathing freq. (n x min.)	-	21.26±6.14	-	23
Heart rate (n x min.)	-	94.53±15.43	-	108
Systolic blood pressure (mm Hg)	-	136.31±22.68	-	109
Diastolic blood pressure (mm Hg)	-	82.37±11.87	-	109
Commorbidities				
Cardiovascular	-	10 (8.93%)	-	112
Cerebrovascular	-	3 (2.68%)	-	112
Diabetes	7 (6.25%)	12 (10.71%)	0.337	224
EPOC	-	8 (7.14%)	-	112
Hypertension	20 (18.02%)	25 (22.32%)	0.526	223
Immunodeficiency	-	6 (5.36%)	-	112
Liver failure: No	-	112 (100.00%)	-	112
Neoplasm	-	6 (5.36%)	-	112
Renal insufficiency	-	5 (4.46%)	-	112
Symptoms				
Clouding of conciousness	-	2 (1.79%)	-	112
Conjunctival congestion	-	1 (0.89%)	-	112
Diarrhea	-	44 (39.29%)	-	112
Disorientation: No	-	112 (100.00%)	-	112
Dry cough	-	74 (66.07%)	-	112
Fatigue	-	63 (56.25%)	-	112
Fever	-	85 (75.89%)	-	112
Headache	-	36 (32.14%)	-	112
Hemoptysis: No	-	112 (100.00%)	-	112
Lymphadenopathy	-	1 (0.89%)	-	112
Myalgia	-	45 (40.18%)	-	112
Nasal congestion	-	7 (6.25%)	-	112
Nausea Vomiting	-	20 (18.02%)	-	111
Odynophagia	-	19 (16.96%)	-	112
Oropharyngeal congestion	-	1 (0.89%)	-	112
Productive cough	-	17 (15.18%)	-	112
Shaking chills	-	25 (22.32%)	-	112
Skin rash	-	3 (2.68%)	-	112
Blood test				
Albumin (g/dL)	-	3.89±0.36	-	64

ALT (U/L)	21.67±11.32	37.82±26.75	<0.001	220
APTT (s)	-	23.23±2.68	-	111
Bilirubin (mg/dL)	0.55±0.27	0.74±0.41	0.160	72
C-reactive protein (mg/L)	-	52.48±58.37	-	112
Creatinine (mg/dL)	0.82±0.17	0.89±0.47	0.144	224
Creatine phosphokinase (U/L)	-	162.12±407.84	-	108
D-dimer (ng/mL)	-	1319.18±6822.22	-	110
Ferritin (ng/mL)	47.29±49.13	579.11±710.03	<0.001	117
Glucose (mg/dL)	89.25±15.33	126.21±105.66	<0.001	224
Interleukin 6 (pg/mL)	-	21.50±26.85	-	10
Lactate dehydrogenase (U/L)	-	298.60±253.94	-	110
Leukocytes (10^9/L)	6.87±1.63	6.53±2.70	0.264	223
Lymphocytes (10^9/L)	2.45±0.75	1.25±0.70	<0.001	224
Monocytes (10^9/L)	0.61±0.17	0.39±0.18	<0.001	224
Neutrophils (10^9/L)	3.56±1.20	5.38±7.80	0.016	223
Platelets (10^9/L)	239.20±51.42	220.15±114.36	0.110	224
Procalcitonin (ng/mL)	-	0.14±0.15	-	45
Protein (g/dL)	-	6.48±0.48	-	65
Prothrombin activity (%)	-	96.79±11.65	-	103
Urea (mg/dL)	-	31.79±19.04	-	112

Table S4. Metrics for the statistical analysis, Related to Figures 1-4. Performance metrics from OPLS-DA through a repeated double cross-validation process, using balanced subcohort. Value columns are the mean value. p-value columns were obtained from permutation tests.

Metric	**Training**		**Validation**	
	Value	***p-value***	***Value***	***p-value***
AUROC	0.980	<0.05	0.967	<0.05
Accuracy	0.925	<0.05	0.911	<0.05
Sensitivity	0.896	<0.05	0.881	<0.05
Specificity	0.955	<0.05	0.941	<0.05

Table S5. Raw spectroscopical data, Related to Transparent Methods and Figures 1-4. The Table has been deposited in Mendeley Data:

Millet, Oscar (2020), “SARS-CoV-2 infection dysregulates the metabolomic and lipidomic profiles of serum. Bruzzone et al.”, Mendeley Data, V1, doi: 10.17632/3h96n97xrb.1

Transparent methods

Patient Recruitment.

All serum samples were provided by the Basque Biobank for research (BIOEF). According to the Declaration of Helsinki principles, all participants in the study provided informed consent to clinical investigations, with evaluation and approval from the corresponding ethics committee (CEIC-E 20-26, 1-2016). All data was anonymized to protect the confidentiality of participants.

The patient cohort (*COVID*; n = 263) presented different symptoms compatible with COVID-19, and had been diagnosed as SARS-CoV-2 positive on nasal swab samples by a RT-PCR assay targeting viral RNA regions encoding the envelope protein E and RNA-dependent RNA polymerase (RNase P). RNA was extracted from samples with the MagNa Pure 96 system (Roche, Penzberg, Germany). As regard the Real-time reverse-transcription PCR a 25 µL reaction contained 5 µL of RNA, 12.5 µL of 2 x reaction buffer provided with Superscript III one step RT-PCR system with Platinum Taq Polymerase (Invitrogen, Darmstadt, Germany; containing 0.4 mM of a 50 mM magnesium sulphate solution (Invitrogen), and 1 µg of nonacetylated bovine serum albumin (Roche). All oligonucleotides were synthesised and provided by Tib-Molbiol (Berlin, Germany). Thermal cycling was performed at 55°C for 10 min for reverse transcription, followed by 95°C for 15 s, 58°C for 30 s using the Applied Biosystems ViiA7 instrument (Applied Biosystems, Hong Kong, China). The patients were in the hospital urgency room at the moment of sample collection and all were *hospitalized* after that, so the hospital diet is not a confounding parameter. The serum samples of the control cohort (*preCOVID*; n = 280) were collected in 2018/2019 in overnight fasting conditions, well before start of the current COVID pandemia, by Osarten Kooperatiba Elkartea (Mondragon Cooperative) as extra aliquots during the routine annual medical tests of their employees in the Basque Country by OSARTEN. Further patient data was also registered, including serum biochemical parameters (Tables S2 and S3) and life style habits (data not shown). Both cohorts were collected within the same geographical region (Basque Country) and handled by the same biobank (Basque Biobank). The procedures, mainly temperature, clotting tube and clotting time, were in principle the same. However, since the patient cohort were collected during the peak of the pandemia, it cannot be assured that all these protocols could be completely abided by the clinicians. For this reason, a second patient cohort (135 additional samples), coming from a second hospital, was analyzed. Since the two hospitals are totally autonomous, the two cohorts represent a perfect set to investigate the variability in terms of sample handling.

***Serum sample preparation for NMR measurements*.**

Samples were stored at -80 °C until measured. The delivered frozen serum sample (500 □L) were individually left to thaw at room temperature during several minutes. NMR samples were then prepared by a SamplePro Tube (Bruker Biospin) robot system for liquid handling with integrated temperature control. Briefly, every sample was automatically mixed with phosphate buffer (containing trimethylsilylpropionic acid-d^4 sodium salt, TSP 0.1 mM, and 10% D_2O) at a 1:1 (v/v) ratio and 600 µL were then filled into a 5 mm NMR tube. After manually shaking every sample for several seconds, the NMR tubes were stored at 5 °C inside a tempered SampleJet automatic sample changer mounted on a 600 MHz IVDr spectrometer (Bruker Biospin, Germany).

Production of recombinant RBD and ELISA.

RBD (aa 319-541) was codon-optimized for expression in human cells. The construct was synthesized by GenScript and subcloned into the pHLsec vector (addgene) at cloning site AgeI and KpnI. In order to enhance the affinity purification, a His6× tag was added at the C terminus of the construct. HEK293F suspension cells (Thermo Fisher Scientific) were transiently transfected and split into 200 ml culture flasks at 0.7 × 10^6 cells per ml. DNA was filtered and mixed (1:1) with transfection reagent FectoPRO (Polyplus Transfections) for 10 min at RT and added to the cells. After incubation at 37 °C, 180 rpm, 8% CO2 in a Minitron Pro shaker (Infors HT) for 7 days, cell cultures were harvested by centrifugation at 4000×g for 30 min, and supernatants were collected and filtered with a 0.22 µm System filter (Corning). Supernatants were passed through a HisTrap Ni-NTA column (GE Healthcare) at 4 ml min−1. Washing was performed with a 10-column volume of 20 mM Tris pH 9.5, 200 mM NaCl, and 4% of elution Buffer (20 mM Tris pH 9.5, 200 mM NaCl, 500 mM imidazole). Fractions containing RBD were eluted, collected, concentrated and separated on a Superdex 200 Increase size exclusion column (GE Healthcare) at 0.7 ml min−1 in 20 mM Tris pH 8.0, 200 mM NaCl buffer.

The ELISA protocol was adapted from a previously established immunoassay. Briefly, 96-well ELISA plates (Nunc Maxisorp) were coated overnight at 4°C with 50 µl of RBD protein at 2ug/ml in PBS (Gibco). Next day, the coating solution was removed and plates were blocked with 3% non-fat milk in PBST (PBS plus 0.1% Tween 20) for 1 hour at RT. Serum samples were inactivated (heating at 56°C for 1 hour) and diluted (1:50) in 1% non-fat milk in PBST, and added to the plates for 2 hours at RT. After three washes with 250 µl PBST in a plate washer (Biotek), the wells were incubated with anti--human IgG-horseradish peroxidase (HRP) conjugated secondary antibody (GenScript) diluted 1:5000 for 1 hour at RT. Plates were washed thrice with PBST, 100 µl of TMB (Thermo Scientific) substrate were added in each well for 3-6 min and the reaction was stopped with 100 µl of Stop Solution (Thermo Scientific). The optical density (OD) was measured at 450 nm in a multimode plate reader (Victor Nivo, PerkinElmer).

***Serum NMR measurements*.**

Before start of the measurements, aliquots (600 µL each) of pooled serum (Inovative Research, Inc) were frozen at -80°C. On each measurement day, 3 of these pooled serum samples were included for quality control (QC). The NMR spectrometer was calibrated daily following strict Standard Operation Procedures (SOPs) to ensure highest spectral quality and reproducibility. Every morning three different calibrations tubes were acquired to check the spectrometer was in optimal conditions. First a temperature calibration tube containing a 99.8% deuterated methanol (MeOD) standard sample in a sealed 5 mm NMR tube was used to calibrate the temperature to ensure that serum samples were run at exactly 310 K. The MeOD NMR tube was inserted into the Sample Track robot and allowed 5 min to equilibrate. After that, an automatically tune and matching was performed, locked to deuterated methanol and automatically shimmed. A standard 90°proton parameter set was used to run an experiment with 2 scans using a pulse length of 1 µs. When the experiment was processed with a line broadening of 3.0 Hz the real probe temperature was able to be calculated by measuring the distance in Hz between the two methanol peaks, The second calibration tube is a standard 2 mM sucrose sample to optimize the water suppression. Different experiments were performed evey day. For all of them the sample was locked to 90% H2O+10% D2O. The lock and shimming were done using the automated routine. The first experiment was done to optimize the offset (O1) by using a 1D NMR experiment with presaturation, a long relaxation delay and 1 scan. After that the water suppression performance is evaluated where the signal-to-noise value must be higher than 310 and (measured on the anomeric proton of sucrose), the splitting lower than 15 % and the water hump measured at 50% not bigger than 30 Hz and measured at 10% lower than 50 Hz. Using a second experiment was calculated the optimal 90° pulse for the sample. The result is optimal when half height of the TSP

peak is < 0.7 Hz with no line broadening). A third tube called Quant Ref was run for quantification purposes and was based on an external reference created by an electronic device. The sample consists several standard metabolites commonly found in biofluids that are stable over the time. A 1D NOESY experiment was performed also every morning using the same parameters used for the samples and the values obtained had to be always into the same range (Dona et al., 2014). All ^{1}H-NMR spectra were measured at 310 ± 0.05 K to identify different lipoprotein subfractions parameters because its success in various epidemiological studies with very large study sizes (Jiménez et al., 2018). The NMR spectrometer was equipped with a BBI probehead with a z-gradient coil and BOSS-III shim system. Four different ^{1}H NMR experiments were recorded per sample: a standard one-dimensional (1D) ^{1}H spectrum (pulseprogram: *noesyphpr1d*) with water presaturation, a (1D) ^{1}H CPMG experiment (pulseprogram: *cpmgpr1d*) implementing a T2 filter to suppress the broad signals of proteins and other macromolecules, a two-dimensional (2D) J-resolved experiment (pulseprogram: *jresgpprqf*) and, for selected samples, also a 2D ^{1}H TOCSY experiment (60 ms DIPSI2 mixing) to assist in metabolite identification. The list of quantified metabolites and lipoprotein subclasses was obtained automatically by B.I.QuantPS 2.0 and B.I.-LISA (Bruker BioSpin), respectively. Quantification of lipoproteins was based on the integration of their bulk–CH3 and –CH2– group signals at 0.8 and 1.25 ppm, respectively that appeared in the 1D ^{1}H NMR spectrum and fitting them using 105 lipoprotein and lipoprotein subclass related parameters (Jiménez et al., 2018). The small metabolites were identified in the one-dimensional spectra using The Human Metabolome Database (HMDB) Version 4.0 and the ChenomX NMR Suite (Chenomx Inc., Edmonton, Canada).

***Detection of multivariate outliers*.**

Each CPMG ^{1}H-NMR spectrum, after automatic processing by Topspin (Bruker Biospin, Germany), was bucketed into consecutive bins of fixed 0.03 ppm width over the region from 0.5 to 9.5 ppm, were the pertaining bin integrals (bin intensities) were obtained as average sums (i.e. by dividing the total bin integral by the number of points in the bin). The spectral region between 4.7 and 5.0 ppm (containing the residual water signal) was excluded, leaving a total of 290 bins ([9.5 – 0.5 – (5.0 – 4.7)] ppm / 0.03 ppm) for analysis. All bin intensities were normalized relative to the total spectrum intensity in order to minimize the effect of different concentrations. After pareto scaling, multivariate DBSCAN (Density-Based Spatial Clustering of Applications with Noise) clustering was used with bin intensities as input variables (Ester et al., 1996). Briefly, this clustering algorithm detects groups of high density (large number of neighbors) considering a multivariate space (bins), where groups with low density or isolated samples are marked as extremes. As further input parameters for the algorithm we set eps = 10 (size of the epsilon neighborhood) and minPts = 5 (number of minimum points in the eps region), and used the dbscan R package (version 1.1-2). DBSCAN was independently applied to the two *COVID* and *preCOVID* groups, where 6 detected outliers from *COVID* cohort were discarded but no one for*preCOVID* group.

***Statistical analysis*.**

Principal Component Analysis (PCA) was used as dimensionality reduction method to facilitate a general overview over both groups (*COVID* and *preCOVID*) via the first and second principal components in score plots, while loadings provided insight into the weights of variables in each component. Separate PCA were performed for the serum metabolites and lipoprotein subclasses. In both cases, the variables were first mean-centered and then divided by their standard deviation. To assess the capacity of metabolomics data in distinguishing COVID-19, an Orthogonal Partial Least-Squares Discriminant Analysis (OPLS-DA) was performed for the full set of serum metabolites and lipoprotein subclasses, after normalizing their values. A repeated double cross validation process (rdCV) (Filzmoser et al., 2009) was used to select the number of

orthogonal components and validate the predictive capacity. Several metrics were averaged through 100 repetitions: Area Under the Receiver Operating Characteristics (AUROC), accuracy, sensitivity and specificity. The outer loop of rdCV performed a 4-fold cross validation process. The inner loop selected the number of orthogonal components (from 1 to 5) based on AUROC in a new 7-fold cross validation process. If AUROC was not improved in at least 5% adding a new orthogonal component, then no more components were added. To measure the statistical significance of calculated metrics, a permutation test (Szymańska et al., 2012) was performed for the whole process. The number of permutations was set to 100. Then, for each permutation, new values for the metrics were obtained. The thresholds for p-values were calculated as the proportion of permuted results that reached a value at least as high as the real one (those obtained from rdCV without permuted labels). In order to visualize OPLS-DA results, a final model was built with all samples and a score plot between the predictive and the orthogonal components was generated. Loadings from OPLS-DA were used to determine those variables with a bigger contribution to the cohort separation. To quantify the metabolic effect of COVID-19, a multivariable linear model was built for each metabolite and lipoprotein subclass, using the metabolite or lipoprotein as dependent variable and the COVID-19 status (*positive* or *control*) as independent variable, adjusted by gender and age because metabolism is deeply affected by those confounding factors (Darst et al., 2019; Rist et al., 2017; Wang et al., 2020). Coefficients and p-values associated with a COVID-19 *positive* variable were extracted from models. For each p-value, the 95% confidence interval was also calculated. Coefficients and intervals were normalized by their standard deviation in the control group to make them comparable between metabolites or lipoproteins. The statistical significance threshold was set to $\alpha = 0.05$ and p-values were adjusted with the False Discovery Rate (FDR) method to control for Type I errors due to multiple comparisons. Individual metabolite or lipoprotein subclass analyses were summarized in forest plots, where each variable is represented by its mean value and 95% confidence interval. All analyses were performed using the R statistical software, version 3.6.0 (http://cran.r-project.org/) and the following R packages: ade4 (version 1.7-15), factoextra (1.05), ggforestplot (0.1.0), ropls (1.16.0), and tidyverse (1.3.0).

Data and Software availability

Table S1 (Concentrations of metabolites and lipoproteins, Related to Figures 3 and Figure 4) and Table S5 (Raw spectroscopical data, Related to Transparent Methods and Figures 1-4), have been deposited in Mendeley Data:

Millet, Oscar (2020), “SARS-CoV-2 infection dysregulates the metabolomic and lipidomic profiles of serum. Bruzzone et al.”, Mendeley Data, V1, doi: 10.17632/3h96n97xrb.1

Supplemental References

Corman, V.M., Landt, O., Kaiser, M., Molenkamp, R., Meijer, A., Chu, D.K., Bleicker, T., Brünink, S., Schneider, J., Schmidt, M.L., et al. (2020). Detection of 2019 novel coronavirus (2019-nCoV) by real-time RT-PCR. Euro Surveill *25*, 2000045.

Darst, B.F., Koscik, R.L., Hogan, K.J., Johnson, S.C., and Engelman, C.D. (2019). Longitudinal plasma metabolomics of aging and sex. Aging *11*, 1262--1282.

Dona, A.C., Jiménez, B., Schäfer, H., Humpfer, E., Spraul, M., Lewis, M.R., Pearce, J.T., Holmes, E., Lindon, J.C., and Nicholson, J.K. (2014). Precision high-throughput proton NMR spectroscopy of human urine, serum, and plasma for large-scale metabolic phenotyping. Analytical chemistry *86*, 9887-9894.

Ester, M., Kriegel, H.-P., Sander, J., and Xu, X. (1996). A Density-Based Algorithm for Discovering Clusters in Large Spatial Databases with Noise. Kdd'96, 226--231.

Filzmoser, P., Liebmann, B., and Varmuza, K. (2009). Repeated double cross validation. Journal of Chemometrics *23*, 160-171.

Jiménez, B., Holmes, E., Heude, C., Tolson, R.F., Harvey, N., Lodge, S.L., Chetwynd, A.J., Cannet, C., Fang, F., Pearce, J.T.M., et al. (2018). Quantitative Lipoprotein Subclass and Low Molecular Weight Metabolite Analysis in Human Serum and Plasma by (1)H NMR Spectroscopy in a Multilaboratory Trial. Analytical chemistry *90*, 11962-11971.

Rist, M.J., Roth, A., Frommherz, L., Weinert, C.H., Krger, R., Merz, B., Bunzel, D., Mack, C., Egert, B., Bub, A., et al. (2017). Metabolite patterns predicting sex and age in participants of the Karlsruhe Metabolomics and Nutrition (KarMeN) study. PloS one *12*, e0183228.

Szymańska, E., Saccenti, E., Smilde, A.K., and Westerhuis, J.A. (2012). Double-check: validation of diagnostic statistics for PLS-DA models in metabolomics studies. Metabolomics : Official journal of the Metabolomic Society *8*, 3-16.

Wang, Y., Wang, G., Jing, R., Hu, T., Likhodii, S., Sun, G., Randell, E., Jia, G., Yu, T., and Zhang, W. (2020). Metabolomics analysis of human plasma metabolites reveals the age- and sex-specific associations. Journal of Liquid Chromatography and Related Technologies *43*, 185-194.